

EPA decoration is essential for virulence

1 **Decoration of the enterococcal polysaccharide antigen EPA is essential for virulence,**
2 **cell surface charge and sensitivity to effector molecules of innate immunity**

3

4

5 Robert E. Smith ^{1,2†}, Bartłomiej Salamaga ^{1,2†}, Piotr Szkuta ^{1,2}, Natalia Hajdamowicz ^{1,2},
6 Tomasz K. Prajsnar ^{1,2}, Gregory Bulmer ^{1,2}, Thierry Fontaine ³, Justyna Kołodziejczyk ^{1,2},
7 Jean-Marie Herry ⁴, Andrea Hounslow ^{1,2}, Mike P. Williamson ^{1,2},
8 Pascale Serror ^{4*} and Stéphane Mesnage ^{1,2*}

9

10

11 ¹ Krebs Institute, University of Sheffield, Firth Court, Western Bank, Sheffield S10 2TN,
12 UK;

13 ² Department of Molecular Biology and Biotechnology, University of Sheffield, Firth Court,
14 Western Bank, Sheffield S10 2TN, UK;

15 ³ Unité des Aspergillus, Institut Pasteur, 75015 Paris, France;

16 ⁴ Micalis Institute, INRA, AgroParisTech, Université Paris-Saclay, 78350 Jouy en Josas,
17 France

18

19

20 † These authors contributed equally to this work

21

22

23 * Corresponding authors

24 Email: s.mesnage@sheffield.ac.uk; pascale.serror@inra.fr

25

26

27

28 **Short title:** EPA decoration is essential for pathogenesis

29

30

31 **Abstract**

32 *Enterococcus faecalis* is an opportunistic pathogen with an intrinsically high resistance to
33 lysozyme, a key effector of the innate immune system. This high level of resistance requires
34 several genes (*oatA*, *pgdA*, *dltA* and *sigV*) acting synergistically to inhibit both the enzymatic
35 and cationic antimicrobial peptide activities of lysozyme. We sought to identify novel genes
36 modulating *E. faecalis* resistance to lysozyme. Random transposon mutagenesis carried out in
37 the quadruple *oatA/pgdA/dltA/sigV* mutant led to the identification of several independent
38 insertions clustered on the chromosome. These mutations were located in a locus referred to as
39 the enterococcal polysaccharide antigen (EPA) variable region located downstream of the
40 highly conserved *epaA-epaR* genes proposed to encode a core synthetic machinery. The *epa*
41 variable region was previously proposed to be responsible for EPA decorations, but the role of
42 this locus remains largely unknown. Here, we show that EPA decoration contributes to
43 resistance towards charged antimicrobials and underpins virulence in the zebrafish model of
44 infection by conferring resistance to phagocytosis. Collectively, our results indicate that the
45 production of the EPA rhamnopolysaccharide backbone is not sufficient to promote *E. faecalis*
46 infections and reveal an essential role of the modification of this surface polymer for
47 enterococcal pathogenesis.

48

49 **Introduction**

50

51 *Enterococcus faecalis* is a commensal bacterium found in the gastro-intestinal tract of
52 humans and frequently isolated from the environment as a result of faecal contamination [1,
53 2]. Although this organism is considered as harmless in healthy carriers, *E. faecalis* has been
54 proposed to contribute to the pathogenesis of inflammatory bowel disease and colorectal
55 cancer [3, 4]. *E. faecalis* can also cause a wide range of hospital-acquired opportunistic
56 infections that can be life-threatening [1]. *E. faecalis* infections can be difficult to treat due to
57 the resistance of this organism to antibiotics such as cephalosporins and glycopeptides
58 (Vancomycin Resistant Enterococci, VRE) and its capacity to form biofilms [5].
59 Interestingly, *E. faecalis* strains responsible for hospital-acquired infections are also found in
60 healthy individuals and genes associated with virulence are not only present in clinical
61 isolates [6]. How this organism can cause infections is therefore not entirely understood. One
62 property of *E. faecalis* that contributes to the onset of infections is its resistance to the host
63 innate immune system. Cell surface polymers including teichoic acids (TAs), a capsule and
64 the enterococcal polysaccharide antigen (EPA) confer phagocytosis evasion and resistance to
65 complement activation [7-9]. *E. faecalis* also displays an intrinsically high resistance to
66 lysozyme, a key component of the innate immune system representing a first line of defence
67 against pathogens. Lysozyme is found in virtually all human biological fluids including
68 saliva, milk, serum and tears where it is found at concentrations between 1-2 mg ml⁻¹ [10,
69 11]. Lysozyme has two distinct antimicrobial activities. Firstly, it hydrolyses the glycan
70 chains of peptidoglycan, the major component of the bacterial cell wall, causing cell lysis
71 [12]. Secondly, lysozyme displays cationic antimicrobial peptide (CAMP) activity. Lysozyme
72 contains highly charged C-terminal sequences (RAWVAWRNR in human lysozyme)
73 sufficient to inhibit bacterial growth [13] by causing membrane permeabilization [14].
74 Four genes (*oatA*, *pgdA*, *dltA* and *sigV*) contribute synergistically to lysozyme resistance in *E.*
75 *faecalis*. Both OatA and PgdA modify peptidoglycan glycan strands, thereby inhibiting
76 lysozyme catalytic activity. OatA is an *O*-acetyl transferase that transfers an acetyl group
77 onto the C6-OH group of *N*-acetylmuramic acid residues [15]. PgdA is produced in response
78 to lysozyme and is an esterase that removes the acetyl group in position 2 of *N*-
79 acetylglucosamine residues [16]. DltA is a D-alanine-D-alanyl carrier ligase essential for the
80 alanylation of TAs. It has been proposed that this modification reduces the net negative
81 charge of TAs and inhibits the CAMP activity of lysozyme [17]. SigV is an extracytoplasmic
82 sigma factor that controls the expression level of *pgdA* in response to lysozyme [18, 19].

EPA decoration is essential for virulence

83 *oatA*, *pgdA*, *dltA* and *sigV* act in concert to confer high-level resistance to lysozyme in *E.*
84 *faecalis*. Deletions in these genes (alone or in combination) have been associated with a
85 reduction in virulence in mice or *Galleria mellonella* [18, 19] and a decrease in survival
86 within murine peritoneal macrophages [15].

87 In this study, we show that the quadruple mutant (*oatA*, *pgdA*, *dltA* and *sigV*; *OPDV* strain)
88 still displays a relatively high resistance to lysozyme in comparison to other Firmicutes.
89 Using transposon mutagenesis, we used this quadruple mutant to carry out transposon
90 mutagenesis and to identify additional genes involved in lysozyme resistance. We show that
91 several genes contributing to the decoration of the enterococcal polysaccharide antigen play
92 an essential role in the resistance to effectors of the innate immune system and in virulence.

93 **Results**

94

95 **The *E. faecalis* quadruple mutant harboring deletions in *oatA*, *pgdA*, *dltA* and *sigV***
96 **displays a relatively high residual resistance to lysozyme.**

97 We determined the minimal inhibitory concentrations (MIC) of lysozyme for several Gram-
98 positive bacteria (Table 1; see S1 Fig for a representative set of MIC assays). *Micrococcus*
99 *luteus*, used as a reference substrate to define lysozyme activity [20] had an expected very
100 low MIC of 5×10^{-4} mg ml⁻¹. MIC values were higher for all Firmicutes tested. Growth of
101 several species was inhibited by lysozyme concentrations of 0.0312 mg ml⁻¹ (*Aerococcus*
102 *viridans* *Bacillus subtilis*, *Bacillus megaterium* and *Lactobacillus cellobiosus*). *Lactococcus*
103 *lactis* growth was inhibited by concentrations of 0.125 mg ml⁻¹. The MIC of lysozyme for all
104 pathogens tested was relatively high: 4 mg ml⁻¹ for *Listeria monocytogenes* and >16 mg ml⁻¹
105 for *Staphylococcus aureus*, and all enterococci and streptococci tested. In *L. monocytogenes*,
106 lysozyme resistance was largely due to peptidoglycan de-*N*-acetylation. Deletion of the gene
107 encoding the deacetylase PgdA led to a 32-fold decrease in resistance (MIC=0.125 mg ml⁻¹).
108 Interestingly, abolishing peptidoglycan *O*-acetylation or de-*N*-acetylation in *E. faecalis* only
109 had a minor impact on lysozyme resistance [16, 19]. The combined deletions in the four
110 genes contributing to *E. faecalis* lysozyme resistance (*oatA*, *pgdA*, *dltA* and *sigV*; *OPDV*
111 strain) was required for 10-fold reduction in the MIC of this antimicrobial compound
112 (0.5 mg ml⁻¹). However, the lysozyme MIC for the *OPDV* mutant was still higher than that of
113 non-pathogenic Gram-positive bacteria.

114

115 **Transposon mutagenesis of the *OPDV epa* variable region confers resistance to**
116 **lysozyme.**

117 The relatively high lysozyme MIC of the quadruple mutant (*OPDV* strain) prompted us to
118 further explore *E. faecalis* properties modulating lysozyme activity. We constructed a
119 transposon mutant library in the *OPDV* background using the *Mariner*-based system
120 previously described for *E. faecium* [21]. Transposon mutants were selected on agar plates
121 containing lysozyme at a concentration of 2 mg ml⁻¹, four times the MIC for the parental
122 *OPDV* strain. Approximately 2×10^5 mutants were plated and after 24 h incubation at 37°C,
123 16 mutants forming colonies at this concentration were isolated and further analysed.

124 Mapping the transposon insertion sites revealed that 9 mutants had insertions downstream of
125 the conserved *epaA-epaR* region encoding the core synthetic apparatus likely required to
126 produce the enterococcal polysaccharide antigen EPA (Fig 1A) [22]. The region containing

EPA decoration is essential for virulence

127 the insertions displays genetic variability between strains and was proposed to be responsible
128 for the decoration of the EPA polysaccharide [22-24]. Mutations were clustered around three
129 genes encoding putative glycosyltransferases and a homolog of *wcaG*, an
130 epimerase/dehydratase (Fig 1B).

131 Transposon mutants were complemented to formally establish that the insertions in the *epa*
132 variable region were responsible for lysozyme resistance. Four plasmids were constructed to
133 express *OG1RF_11720*, *OG1RF_11715* (*epaOX*), *OG1RF_11714* (*epaX-like*) and
134 *OG1RF_11707* under the control of the inducible *tet* promoter. Following transformation into
135 *E. faecalis*, gene expression was induced in the presence of anhydrotetracycline (ATc) and
136 the production of his-tagged proteins was checked by western blot (S2 Fig).
137 Complementation was evaluated by measuring susceptibility to lysozyme (Fig 2). Lysozyme
138 resistance associated with transposon insertions in genes *OG1RF_11720*, *OG1RF_11715*,
139 *OG1RF_11714* and *OG1RF_11707* could be complemented when the disrupted gene was
140 expressed *in trans*. By contrast, the parental susceptibility to lysozyme could not be restored
141 when complementation experiments were carried out with plasmids encoding a gene distinct
142 from the one disrupted (Table 2). Altogether, these experiments confirmed that the resistance
143 phenotypes of the mutants analysed were due to the disruption of the genes indicated in Fig 1.

144

145

146 **Mutations in the *epa* variable region alter the negative surface charge of *E. faecalis* and** 147 **are associated with minor changes in sugar composition.**

148 The impact of *epa* transposon insertions on the production of EPA was investigated.
149 Polysaccharides were extracted from cultures at the end of exponential growth as previously
150 described [25]. Similar amounts of EPA were extracted as assessed by neutral sugar assays
151 and dry weight (between 20 and 30 mg l⁻¹). Each purified EPA sample was run on a
152 polyacrylamide gel and stained with the cationic dye alcian blue (Fig 3A). Whilst *OG1RF*
153 and *OPDV* polysaccharide bands previously named PS1 and PS2 were present [8], these were
154 not detected in mutant samples, possibly because the reduced negative charge no longer
155 allowed EPA to migrate in the gel or no longer allowed these polymers to be stained by
156 alcian blue. As expected, complementation restored the detection of EPA after staining by
157 alcian blue (Fig 3A).

158 We tested the impact of the transposon insertions on EPA charge by measuring the
159 electrophoretic mobility of *E. faecalis* cells using micro-electrophoresis, which allows single
160 particle tracking (Fig 3B) [26]. *OG1RF* cells displayed a negative electrophoretic mobility

EPA decoration is essential for virulence

161 (migration towards the anode), even at low pH, indicating a negative surface charge. Despite
162 the increased susceptibility of *OPDV* cells to lysozyme, the electrophoretic mobility
163 measured with this strain was not significantly different from the mobility of OG1RF cells at
164 all pHs tested (Fig 3B; S1 and S2 Table). Three of the four insertion mutants
165 (*OPDV_11720::Tn2.5*, *OPDV_11715::Tn2.13* and *OPDV_11720::Tn2.8*) displayed similar
166 electrophoretic mobilities, very distinct from the parental *OPDV* strain. The negative surface
167 charge of these mutants was significantly reduced as compared to that of the parental *OPDV*
168 strain (**** $P < 0.0001$ for all pH conditions), the difference being most prominent at pH 3.0
169 (Fig 3B). As expected, differences between *OPDV*, *OPDV_11720::Tn2.5*,
170 *OPDV_11715::Tn2.13* and *OPDV_11720::Tn2.8* cells were abolished when the mutations
171 were complemented. Mutant *OPDV_11714::Tn2.14* only showed a difference with the
172 parental *OPDV* strain at pH 2.0 (**** $P < 0.0001$). This difference was no longer detected
173 when the mutation was complemented.

174 Previous studies reported the presence of phosphate in the EPA polysaccharide [25].
175 Phosphate assays carried out on purified EPAs revealed a significantly lower phosphate
176 content for all transposon mutants as compared to the parental strain (Fig 3C and S3 Table),
177 suggesting that the genes from the *epa* variable region are at least in part involved in the
178 addition of phosphate in this polymer. Collectively, our experiments revealed that several
179 genes in the *epa* variable region contribute to the negative charge of *E. faecalis* cell surface.

180 To confirm that the lack of detection of EPA on polyacrylamide gels was due to a loss of
181 negatively charged groups rather than a lack of rhamnopolysaccharide production, we carried
182 out carbohydrate composition analyses on purified EPA. As anticipated, EPA composition
183 was very similar in OG1RF and *OPDV* strains; rhamnose, glucose, *N*-acetylglucosamine
184 (GlcNac) and *N*-acetylgalactosamine (GalNac) accounted for approximately 95% of the
185 sugars identified (*ca.* 30%, 30%, 20% and 15%, respectively) and galactose was found in
186 limited amounts (5%). The proportion of glucose and GlcNac remained similar to parental
187 *OPDV* levels in all *epa* mutants, whilst both GalNac and galactose amounts decreased to an
188 increase of rhamnose. Interestingly, these changes were different depending on the mutant
189 considered. For example, EPA extracted from *OPDV_11718::Tn2.8* was the only mutant
190 EPA that still contained some galactose. The relative proportion of rhamnose increased in all
191 mutants. GalNac content decreased dramatically in all mutant EPA and could not be detected
192 in *OPDV_11715::Tn2.13*.

193

EPA decoration is essential for virulence

194 **NMR analyses reveal that the *epa* variable region contributes to minor modifications of**
195 **the EPA polysaccharide.**

196 To gain further insight into the contribution of *epa* variable genes to the structure of EPA, we
197 carried out NMR analyses on purified polysaccharides. The 1D proton NMR spectra of all
198 polysaccharides were overall similar but mutations in the *epa* variable region were associated
199 with modifications in the anomeric region (Fig 4A). Clear differences were also detected in
200 the relative intensities of methyl protons in the mutant spectra. For all mutants, the intensity
201 of *N*-acetyl signals (1.9-2.2 ppm) decreased whilst the intensity of methyl protons
202 corresponding to rhamnose residues (1.2-1.6 ppm) increased, suggesting a lower content of
203 hexosamine in mutant EPAs and a relative increase of rhamnose. This result is in agreement
204 with the carbohydrate analyses following acid hydrolysis (Fig 3D and S3 Fig). ¹H-¹³C HSQC
205 spectra revealed that EPA has a very complex structure, as evidenced by the detection of over
206 30 signals in the anomeric region (Fig 4B). The comparison of 2D spectra corresponding to
207 *OPDV* and mutant polysaccharides revealed that each *epa* mutation only led to a limited
208 number of changes including changes in the signal intensity, signal shifts and disappearance
209 (S4 Fig). The number and the nature of the signals affected in the *epa* mutants were different
210 depending on the mutation considered. Altogether, NMR and sugar analyses supported the
211 idea that the *epa* variable genes are involved in limited modifications of the EPA
212 rhamnopolysaccharide previously described as “decorations”.

213

214 **Epa decoration determines susceptibility to antimicrobials targeting the cell envelope.**

215 All *epa* transposon insertions were combined with four other mutations present in the in
216 *OPDV* strain (*oatA*, *pgdA*, *dltA* and *sigV*), leaving the possibility of epistatic interactions
217 between these mutations. To avoid this potential issue, we built in-frame *epa* deletions in the
218 OG1RF genetic background (S5 Fig) before testing the impact of EPA decorations on
219 resistance to antimicrobials targeting the cell envelope (Fig 5). All *epa* mutants were more
220 sensitive to SDS than OG1RF, mutants $\Delta 11714$ and $\Delta 11707$ being less sensitive than the two
221 others. Interestingly, mutant $\Delta 11714$ ($\Delta epaX$ -like) was the only one that did not display
222 increased susceptibility to sodium cholate, a primary bile salt. Mutant $\Delta 11720$ was the only
223 one with an increased susceptibility to both polymyxin B and nisin, two cationic peptides
224 targeting the cell envelope. Mutants $\Delta 11707$ and $\Delta 11715$ were more susceptible to polymyxin
225 B than the wild-type strain, but barely more susceptible to nisin. Finally, deletion of

EPA decoration is essential for virulence

226 *OG1RF_11714* had no detectable impact on resistance to either of the CAMPs tested. Taken
227 together, these results indicated that genes in the *epa* variable region are required for
228 resistance to antimicrobials targeting the cell envelope.

229

230 **The decoration of the EPA rhamnopolysaccharide is essential for virulence and** 231 **underpins phagocyte evasion.**

232 The impact of *epa* mutations on *E. faecalis* virulence was tested in the zebrafish experimental
233 model of infection (Fig 6). Cell suspensions corresponding to approximately 1,200 CFUs
234 were injected in the bloodstream of LWT embryos 30 h post fertilization (hpf) and the
235 survival of larvae was monitored for 90 h post infection (hpi). As a preliminary experiment,
236 we analysed the virulence of the *OPDV* transposon mutants (S6 Fig). Each *epa* transposon
237 mutant had a significantly reduced virulence as compared to the wild-type OG1RF strain.
238 Even though the combined deletions in *oatA*, *pgdA*, *dltA* and *sigV* did not impair the
239 virulence of *E. faecalis* in the zebrafish model of infection (S7 Fig), we could not exclude the
240 possibility of an epistatic relation between the *OPDV* and *epa* mutations. We therefore
241 repeated the zebrafish infections using the in-frame *epa* deletion mutants in the wild-type
242 OG1RF genetic background (S5 Fig). All *epa* mutants showed a significant decrease in
243 virulence as compared to the wild-type OG1RF (Fig 6), killing only between 0-10% of the
244 larvae as opposed to the 40 to 55% of killing following injection of the wild-type strain; Fig
245 6A-D). As expected, the complementation of each *epa* deletion fully restored the virulence.
246 Although the *epa* deletion mutants (except the $\Delta epaX$ -like strain) present a slight defect in
247 their growth rate, it is unlikely that this accounts for the lack of virulence; all complemented
248 strains (and the wild-type OG1RF harbouring an empty complementation vector) also present
249 a growth defect (S8 Fig) and yet kill zebrafish larvae as well as the wild-type strain (Fig 6).

250 The production of EPA has been associated with an increased resistance to phagocytosis,
251 which represents a key step during pathogenesis [8, 27]. We therefore quantified
252 phagocytosis in zebrafish larvae infected with the wild-type OG1RF and one representative
253 *epa* mutant (*OG1RF_Δ11714*, *epaX*-like) expressing the red fluorescent protein mCherry (Fig
254 7). Confocal microscopy images were used to measure bacterial uptake by phagocytes
255 labelled with anti L-plastin antibodies coupled to Alexa-488, a green fluorophore, as
256 previously described [28]. The ratio between red fluorescence inside to red fluorescence
257 outside phagocytes was significantly higher for the *epaX*-like mutant (*OG1RF_Δ11714*) than
258 for the wild-type strain (***P*=0.0006) or the complemented strain (OG1RF $\Delta 11714$ +

EPA decoration is essential for virulence

259 pTetH-*OGIRF_11714*; ** $P = 0.0049$). As expected, no difference in phagocytosis was
260 observed between the wild-type and complemented strains (ns, $P > 0.05$) (Fig 7A).
261 Representative pictures shown in Fig 7B-D clearly indicate that unlike the wild-type strain,
262 the *epaX-like* mutant was no longer able to evade phagocytes.

263 Altogether, our data therefore indicate that decoration of the EPA polysaccharide is essential
264 for *E. faecalis* pathogenesis.

265

266 Discussion

267 Previous studies revealed that *E. faecalis* resistance to lysozyme is unusually complex and
268 results from several mechanisms acting synergistically. These include peptidoglycan *O*-
269 acetylation and de-*N*-acetylation, D-alanylation of teichoic acids and transcriptional control
270 by the extracytoplasmic sigma factor SigV. Despite a 100-fold decrease as compared to the
271 wild-type strain, the residual resistance of the quadruple *OPDV* mutant is still relatively high
272 (MIC=0.5 mg ml⁻¹) as compared to other Firmicutes. This result contrasts with other bacteria
273 in which a limited number of genes play a key role in resistance. For example, the combined
274 deletions of *oatA* and *dltA* in *S. aureus* led to a decrease of at least 2,000-fold in resistance as
275 compared to parental strain [13]. Deletion of *pgdA* alone in *L. monocytogenes* is associated
276 with a 32-fold decrease resistance.

277 Using random transposon mutagenesis, we showed that several genes located downstream the
278 conserved *epaA-epaR* region modulate susceptibility to lysozyme. It was proposed that *epaA*-
279 *epaR* encode a core synthetic machinery whilst downstream genes contribute to the
280 decoration of EPA rhamnopolysaccharide [22, 24]. In agreement with previous studies, three
281 distinct polysaccharide bands (named PS1, PS2 and PS3) were detected on polyacrylamide
282 gels ([8] and Fig 3A). The two upper bands simultaneously disappeared in all the transposon
283 mutants, suggesting that both are structurally related to EPA. The nature of the third band is
284 unknown and could be either a metabolic intermediate of EPA or an unrelated polymer. The
285 lack of detection of PS1 and PS2 in EPA polysaccharides from mutants suggested that either
286 their charge did not allow them to enter the gel and/or that they were no longer stained by the
287 cationic dye alcian blue. A similar result was previously described for mutants harbouring
288 deletions in *OGIRF_11715* (*epaOX*) [23] and the homolog of *OGIRF_11714* in V583 (*epaX*)
289 [24]. By comparing the electrophoretic mobility of the transposon mutants to that of the
290 parental *OPDV* strain, we confirmed that the *epa* genes downstream of the *epaA-epaR* locus
291 contribute to the negative charge of the EPA polysaccharide. This negative charge is at least
292 in part due to the presence of phosphate in the polymer. Interestingly, the *OGIRF* and *OPDV*

EPA decoration is essential for virulence

293 strains displayed similar electrophoretic mobilities. Previous studies also showed that
294 alanylation of teichoic and/or lipoteichoic acids in *L. lactis* had no detectable impact on the
295 electrophoretic mobility of this organism [29]. The *dlt* operon has been shown to modify
296 lipoteichoic acids [17]. Since these polymers are embedded inside the cell wall, it is likely
297 that their modification does not lead to a change in the bacterial surface charge. Further
298 experiments are required to test whether alanylation of cell wall polymers only has a
299 moderate impact on the charge of the cell wall or if such modifications can simply not be
300 detected by measuring electrophoretic mobility. Three of the mutants identified in this work
301 carry a transposon in genes encoding putative glycosyl transferases. Despite the low amino
302 acid identity between the glycosyl transferase sequences (19-27% depending on the
303 comparison), these proteins have very similar predicted secondary structures, with two
304 transmembrane domains and both the N- and C-termini exposed at the cell surface. Tertiary
305 structure predictions suggest that all 3 proteins have a very similar fold and are GalNAc
306 transferases. These predictions are in agreement with our NMR and sugar analyses indicating
307 that EPA polysaccharides from all glycosyl transferase mutants (*OPDV_11720*,
308 *OPDV_11715* and *OPDV_11714*) contain less GalNAc and less intense *N*-acetyl proton
309 signals. In addition to a reduced amount of GalNAc, EPA polymers from the glycosyl
310 transferase mutants also contained a reduced amount of galactose. Further analyses are
311 required to explore the catalytic activity of these glycosyl hydrolases. It remains unclear
312 whether they can use distinct sugars as a substrate or if the addition of GalNAc is required for
313 the activity of other glycosyl transferases adding Gal residues. Since none of the heterologous
314 complementations of the transposon mutants were able to restore the parental phenotype, we
315 anticipate that the 3 glycosyl transferases identified play distinct roles. This idea is supported
316 by several independent observations: (i) mutants *OPDV_11720::Tn2.5*,
317 *OPDV_11715::Tn2.13* and *OPDV_11714::Tn2.14* present distinct alterations in their EPA
318 carbohydrate compositions and the deletion mutants present differences in their antimicrobial
319 susceptibility profiles; (ii) 2D-NMR spectra indicate that each mutation is associated with
320 distinct modifications of the signals in the anomeric region; (iii) the *OPDV_11714::Tn2.14*
321 (*epaX-like*) mutant behaved differently from the other *epa* mutants studied since it displayed
322 a less pronounced defect in surface charge. Altogether, our results suggest that
323 glycosyltransferases in the *epa* variable region fulfil distinct roles. The complexity of EPA
324 structure precludes any conclusion about the specific role of individual *epa* genes. However,
325 based on the 2D NMR spectra, it is tempting to assume that *OGIRF_11720*, the first gene of

EPA decoration is essential for virulence

326 the *epa* variable region encodes a glycosyl transferase that is adding the entire EPA
327 decorations, whilst EpaOX and EpaX contribute to the transfer of smaller decorations.
328 *epa* deletion mutants displayed distinct resistance to antimicrobials targeting the cell
329 envelope. Deletion of *OG1RF_11720*, which had the most pronounced impact on EPA
330 structure led to the most pronounced increased susceptibility to antimicrobials. Deletion of
331 *OG1RF_11714* (*epaX*), which had the least pronounced impact on EPA structure only led to
332 an increased susceptibility to SDS. Since *epa* mutations could confer resistance to both
333 negatively charged antimicrobials and CAMPs, these results suggested that the charge of
334 EPA does not entirely account for the resistance to these compounds. We therefore speculate
335 that EPA decorations are critical to maintain cell integrity, as previously suggested [23, 24].
336 A contribution of *epa* decoration genes in biofilm formation [30], resistance to antimicrobials
337 [23] and colonisation [24] was previously suggested, but no information was available on a
338 potential role in the context of pathogeny. *E. faecalis* pathogenesis in the zebrafish model of
339 infection involves two critical steps: phagocyte evasion and tissue damage caused by the
340 metalloprotease GeIE [27]. Since *oatA*, *pgdA*, *dltA* and *sigV* are unlikely to contribute to these
341 processes, it was expected that their simultaneous deletion would have a very limited impact
342 on virulence. By contrast, EPA has been reported to mediate resistance to phagocytic killing
343 [8] and plays a critical role in virulence both in experimental mouse and zebrafish infections
344 [27, 31]. We therefore hypothesized that *epa* mutations altering the decoration of EPA would
345 impair virulence. In agreement with this hypothesis, all *epa* transposon mutants (in the *OPDV*
346 background) and in-frame deletions in the wild-type *OG1RF* background were avirulent in
347 the zebrafish model of infection. Further investigations revealed that the *epaX* mutation leads
348 to a significant increase in *E. faecalis* uptake by phagocytes, suggesting that the decoration of
349 EPA mediates immune evasion and underpins virulence.

350 Collectively, the results provide a paradigm shift in our understanding of *E. faecalis*
351 pathogenesis, revealing that the modifications of EPA, rather than EPA backbone itself,
352 underpin phagocyte evasion, an essential step during host infection. Whether *epa* is directly
353 recognized by the host immune system or is shielding other surface components remains an
354 open question.

355

356 **Materials and methods**

357

358 **Ethics statement**

359 Animal work was carried out according to guidelines and legislation set out in UK law in the
360 Animals (Scientific Procedures) Act 1986 under Project License P1A417A5E. Ethical
361 approval was granted by the University of Sheffield Local Ethical Review Panel.

362

363 **Bacterial strains, plasmids and growth conditions.**

364 Bacterial strains, plasmids and oligonucleotides used in this study are described in S4 Table.
365 All strains were routinely grown at 37°C in Brain Heart Infusion (BHI) broth or BHI-agar
366 1.5 % (w/v) plates unless otherwise stated. For *E. coli*, erythromycin was added at a final
367 concentration of 200 µg ml⁻¹ to select pTetH derivatives. When necessary, *E. faecalis* was
368 grown in the presence of 10 µg ml⁻¹ chloramphenicol, 128 µg ml⁻¹ gentamicin or 30 µg ml⁻¹
369 erythromycin. For complementation experiments, anhydrotetracycline was used at a final
370 concentration of 10 ng ml⁻¹ to induce gene expression.

371

372 **Construction of the *OPDV* strain.**

373 The work describing the contribution of *oatA*, *pgdA*, *dltA* and *sigV* to lysozyme resistance
374 was carried out using *E. faecalis* JH2-2 as a genetic background [16, 19]. Since this
375 laboratory strain is avirulent in the zebrafish model of infection, we decided to use OG1RF as
376 a parental strain [32]. The quadruple OG1RF mutant harbouring deletions in *oatA*, *pgdA*, *dltA*
377 and *sigV* was built using existing plasmids (S4 Table) to create in-frame deletions in the
378 following order: *oatA*, *pgdA*, *dltA* and *sigV*.

379

380 **Transposon mutagenesis.**

381 A *Mariner*-based transposon mutagenesis system previously described was used [21].
382 Plasmid pZXL5 was introduced in *E. faecalis* *OPDV* by electroporation and transformants
383 were selected at 28°C on plates containing chloramphenicol and gentamicin. Cells harbouring
384 pZXL5 were grown to mid-exponential phase at 28°C and transposition was induced by
385 addition of nisin (25 ng ml⁻¹). The culture was then transferred to 42°C overnight to counter-
386 select the replication of the plasmid. The library was then amplified by growing the cells at
387 42°C in the presence of gentamicin.

388

389 **Transposon mutagenesis.**

EPA decoration is essential for virulence

390 A *Mariner*-based transposon mutagenesis system previously described was used [21].
391 Plasmid pZXL5 was introduced in *E. faecalis* OPDV by electroporation and transformants
392 were selected at 28°C on plates containing chloramphenicol and gentamicin. Cells harbouring
393 pZXL5 were grown to mid-exponential phase at 28°C and transposition was induced by
394 addition of nisin (25 ng ml⁻¹). The culture was then transferred to 42°C overnight to counter-
395 select the replication of the plasmid. The library was then amplified by growing the cells at
396 42°C in the presence of gentamicin.

397

398 **Isolation of transposon mutants resistant to lysozyme.**

399 Serial dilutions of the transposon library were plated on BHI agar plates containing 1, 2 or 4
400 times the lysozyme MIC for the OPDV strain (0.5 mg ml⁻¹) and gentamicin. After 24 to 48 h
401 at 42°C, individual colonies growing at the highest concentration (2 mg ml⁻¹) were chosen for
402 further characterisation.

403

404 **Mapping transposition sites.**

405 Transposon insertion sites were mapped by reverse PCR using two divergent primers
406 (Mar_up and Mar_dn) on the transposon (S9A Fig). Chromosomal DNA was extracted using
407 the Promega Wizard kit and digested by SspI in a final volume of 30 µl at a concentration of
408 4 ng µl⁻¹ (S9B Fig). Digestion products were further diluted to 1 ng µl⁻¹ and self-ligated at
409 16°C for 16 h after addition of 100 U of T4 DNA ligase (NEB) (S9C Fig). Three microliters
410 of the ligation product were used as a template for PCR amplification using oligonucleotides
411 Mar_up and Mar_dn (S9D Fig). PCR products were gel extracted and sequenced using
412 oligonucleotide T7 (S9E Fig). The insertion site was defined as the first nucleotide of the *E.*
413 *faecalis* OG1RF genome immediately downstream of the inverted repeat sequence flanking
414 the transposon.

415

416 **Construction of complementation plasmids.**

417 DNA fragments encoding OG1RF_11720, OG1RF_11715, OG1RF_11714 and
418 OG1RF_11707 were amplified by PCR using the oligonucleotides described in S4 Table.
419 PCR products were digested by NcoI and BamHI and cloned into pTetH, a pAT18 derivative
420 allowing anhydrotetracycline-inducible expression (S. Mesnage, unpublished). Each open
421 reading frame was fused to a C-terminal 6-Histidine tag.

422

423 **Antimicrobial assays.**

EPA decoration is essential for virulence

424 Colonies from a BHI agar plate were resuspended in PBS and diluted to an OD of 1 at
425 600 nm. Ten-fold dilutions were prepared in PBS and 1.5 μ l of each cell suspension were
426 spotted on BHI agar containing antimicrobials at various concentrations. MICs of lysozyme
427 were defined as the concentration of antimicrobial inhibiting the growth of 1.5 μ l of a cell
428 suspension corresponding to a 1000-fold dilution of the cell suspension at OD of 1 at 600 nm.
429 For complementation experiments, anhydrotetracycline was added at a final concentration of
430 10 ng ml⁻¹. At least two biological replicates were carried out for each susceptibility assay.

431

432 **Measurement of electrophoretic mobility.**

433 An overnight culture was diluted 1000-fold in 25 ml of BHI broth and grown for 17 h at 37°C
434 in static conditions. Anhydrotetracycline (100 ng ml⁻¹) was added to all cultures to induce
435 gene expression for complementation and exclude the possibility that this chemical could
436 account for differences between strains. Cells were harvested by centrifugation (5 min,
437 8,000 x g at room temperature), washed twice in 25 ml of 1.5 mM NaCl and resuspended at a
438 concentration of 3.10⁷ CFU ml⁻¹ in 1.5 mM NaCl at various pHs. The electrophoretic mobility
439 was measured in an electric field of 8V cm⁻¹ using a laser zetaphoremeter (CAD
440 Instrumentation, Les Essarts le Roy, France). For each measurement, results were based on
441 the analysis of 200 individual particles. The results presented in Fig 3, S1 and S2 Tables are
442 the combined results of three independent experiments (biological replicates).

443

444 **NMR.**

445 NMR experiments were conducted on a Bruker DRX-600 (plus cryoprobe) spectrometer at
446 25°C. EPA polysaccharides were freeze-dried and resuspended in D₂O. Spectra were
447 processed and analysed using TOPSPIN (version 2.1). Trimethylsilylpropanoic acid was used
448 as a reference.

449

450 **Carbohydrate extraction and analyses.**

451 EPA was extracted as previously described from standing cultures in BHI at the end of
452 exponential growth (OD_{600nm}=0.8) [25]. The method previously described to analyse
453 pneumococcal polysaccharides and conjugates was followed, with the exception of the first
454 acid hydrolysis step [33] Briefly, purified EPA polysaccharides were hydrolyzed in 4 N
455 trifluoroacetic acid for 4 h at 100°C. Hydrolysis products were analysed by high-performance
456 anion-exchange chromatography (HPAEC) coupled to pulsed-amperometric detection (PAD)
457 using a Dionex DX 500 BioLC system (ThermoFisher). Monosaccharides were separated on

EPA decoration is essential for virulence

458 a Carbowac PA10 (4 mm × 250 mm) analytical column (ThermoFisher Scientific) at a flow
459 rate of 1 ml min⁻¹. Solvent A was 18 mM NaOH, solvent B was 100 mM NaOH, and solvent
460 C was 100 mM NaOH containing 1 M sodium acetate. NaOH and NaAc gradients were used
461 simultaneously to elute the carbohydrates by mixing the three eluents. The gradients used
462 were as follows: after 15 min of isocratic elution in buffer A, a 3 min gradient to 100 % of
463 buffer B was applied. A second gradient was applied between 18 and 35 min using buffer C
464 to reach 300 mM sodium acetate. The column was re-equilibrated in 18 mM NaOH for 20
465 min after every run. The following pulse potentials and durations were used: $E1 = 0.1V$, $t1 =$
466 400 ms ; $E2 = -2V$, $t2 = 20\text{ ms}$; $E3 = 0.6V$, $t3 = 10\text{ ms}$; $E4 = -0.1V$, $t4 = 70\text{ ms}$. Data were
467 collected and analysed on computers equipped with the Dionex PeakNet software.
468 Carbohydrate analyses were made in triplicate using three independent EPA extractions from
469 3 distinct colonies.

470

471 **Phosphate assays.**

472 Phosphate content was determined as described previously [34]. 30 µl of 10 % (m/v)
473 Mg(NO₃)₂ in 35 % (v/v) methanol was added to 120 µl containing EPA samples at a
474 concentration of 1 mg ml⁻¹ in pyrex test tubes. After drying the organic material over a
475 flame, 600 µl of 0.5 N HCl was added and the sample was heated for 15 min at 100°C. At
476 this stage, 1.4 ml of a mixture containing a 1:6 ratio of 10 % (m/v) ascorbic acid and 0.42 %
477 (m/v) of (NH₄)₂MoO₄•H₂O in 1 N H₂SO₄ was added. Absorbance at 820 nm was read after
478 an incubation of 1 h at 37°C and phosphate content was determined in reference to a solution
479 of inorganic phosphate.

480

481 **Construction of pGhost derivatives for allele replacement**

482 All plasmids for allele replacement were constructed with the same strategy. Two homology
483 regions were amplified: the 5' homology region (referred to as H1) was amplified with
484 oligonucleotides H11 (sense) and H12 (antisense). The 3' homology region (referred to as
485 H2) was amplified with oligonucleotides H21 (sense) and H22 (antisense). Both PCR
486 products were purified, mixed in an equimolar ratio and fused by overlap extension using
487 oligonucleotides H11 and H22 [35]. The assembled PCR fragment flanked by two restriction
488 sites was digested and cloned into pGhost9 [36] similarly digested. Oligonucleotide
489 sequences and restriction sites used for cloning are described in S4 Table.

490

491 **Construction of *E. faecalis* OG1RF in-frame *epa* mutants**

EPA decoration is essential for virulence

492 Isogenic derivatives of *E. faecalis* OG1RF were constructed by allele exchange using the
493 procedure previously described [37]. Briefly, pGhost9 derivatives were electroporated into
494 OG1RF and transformants were selected at a permissive temperature (28°C) on BHI plates
495 with erythromycin. To induce single crossover recombination, transformants were grown at a
496 non-permissive temperature (42°C) in the presence of erythromycin. The second
497 recombination event leading to plasmid excision was obtained after 5 serial subcultures at
498 28°C without erythromycin. The last overnight subculture was plated at 42°C without
499 erythromycin. A clone harboring a double crossover mutation was identified by PCR (S5 Fig)
500 and further confirmed by sequencing of the recombined region.

501

502 **Zebrafish strains and maintenance.**

503 London wild type (LWT) zebrafish were provided by the aquarium facility at the University
504 of Sheffield. Embryos were maintained in E3 medium at 28°C according to standard
505 procedures previously described [38].

506

507 **Microinjections of *E. faecalis* in zebrafish embryos.**

508 Cells were grown to mid-exponential phase ($OD_{600nm} \sim 0.3$) and harvested by centrifugation
509 (5,000 x g for 10 min at room temperature). Bacteria were resuspended in filtered phosphate
510 buffer saline (150 mM Na_2HPO_4 , 20 mM KH_2PO_4 , 150 mM NaCl [pH 7.5], PBS) and
511 transferred to microcapillary pipettes. Embryos at 30 h post fertilization (hpf) were
512 anaesthetized, dechorionated, embedded in 3 % (w/v) methylcellulose and injected
513 individually with 2 nl of a cell suspension corresponding to *ca.* 1,000 cells as previously
514 described [27]. The number of cells injected was checked before and after each series of
515 injections with a given strain. Zebrafish embryos were monitored at regular intervals until
516 90 h post infection (hpi). At least 20 embryos per group were used.

517

518 **Imaging of infected larvae by confocal microscopy and quantification of uptake by** 519 **phagocytes.**

520 Immuno-labelled embryos were immersed in 0.8 % (w/v) low melting point agarose in E3
521 medium and mounted flat on FluoroDishTM (World Precision Instruments Inc.). Images were
522 collected using a DMI8 confocal microscope (Leica). Image acquisition was performed with
523 the Volocity software and the images were processed with ImageJ 1.49v software. Bacterial
524 phagocytosis was quantified using an ImageJ custom script called Fish Analysis, which can
525 be obtained from <http://sites.imagej.net/Willemsejj/> or via ImageJ updater. All bacteria were

EPA decoration is essential for virulence

526 identified based on their fluorescence (mCherry, Channel 2). Subsequently, the fluorescence
527 intensity of the phagocytes (Alexa 488, Channel 1) surrounding the phagocytosed bacteria
528 was measured. The phagocytosed bacteria had high fluorescence intensity of Channel 2 and
529 low fluorescence intensity of Channel 1. The area of phagocytosed bacteria was compared
530 with the area of non-phagocytosed bacteria and their ratio was calculated.

531

532 **Statistical analyses.**

533 Statistical analyses were performed using GraphPad Prism version 7.03. Comparisons
534 between survival curves were made using the log rank (Mantel-Cox) test. Electrophoretic
535 mobilities were compared using two-way ANOVA. Phosphate contents were compared using
536 an unpaired *t*-test with Welch's correction. Comparison of uptake by zebrafish macrophages
537 was carried out using an unpaired non-parametric Dunn's multiple comparison test.

538

539

540 **Acknowledgments**

541 The authors would like to thank Abdellah Benachour (University of Caen) for providing the
542 plasmids used to construct the *OPDV* strain and the Bateson Centre aquaria staff for their
543 assistance with zebrafish husbandry. The authors thank Dr Philip Elks for access to the
544 confocal microscope and Paul Martin (University of Bristol) for the kind gift of anti L-plastin
545 antibodies.

References

546

547

548

549

550

551

552

553

554

555

556

557

558

559

560

561

562

563

564

565

566

567

568

569

570

571

572

573

574

575

576

577

578

579

580

581

582

583

584

585

586

587

588

589

590

591

592

593

594

595

596

597

598

599

1. Arias CA, Murray BE. The rise of the *Enterococcus*: beyond vancomycin resistance. *Nat Rev Microbiol.* 2012;10(4):266-278. doi: 10.1038/nrmicro2761. pmid: 22421879.
2. Sassoubre LM, Ramsey MM, Gilmore MS, Boehm AB. Transcriptional response of *Enterococcus faecalis* to sunlight. *J Photochem Photobiol B.* 2014;130:349-356. doi: 10.1016/j.jphotobiol.2013.12.013. pmid: 24434819.
3. Ocvirk S, Sava IG, Lengfelder I, Lagkouvardos I, Steck N, Roh JH, et al. Surface-associated lipoproteins link *Enterococcus faecalis* virulence to colitogenic activity in IL-10-deficient mice independent of their expression levels. *PLoS Pathog.* 2015;11(6):e1004911. doi: 10.1371/journal.ppat.1004911. pmid: 26067254.
4. Wang X, Yang Y, Huycke MM. Microbiome-driven carcinogenesis in colorectal cancer: Models and mechanisms. *Free Radic Biol Med.* 2017;105:3-15. doi: 10.1016/j.freeradbiomed.2016.10.504. pmid: 27810411.
5. Hancock LE, Perego M. Systematic inactivation and phenotypic characterization of two-component signal transduction systems of *Enterococcus faecalis* V583. *J Bacteriol.* 2004;186(23):7951-7958. pmid: 15547267.
6. Guzman Prieto AM, van Schaik W, Rogers MR, Coque TM, Baquero F, Corander J, et al. Global emergence and dissemination of enterococci as nosocomial pathogens: attack of the clones? *Front Microbiol.* 2016;7:788. doi: 10.3389/fmicb.2016.00788. pmid: 27303380.
7. Geiss-Liebisch S, Rooijackers SH, Beczala A, Sanchez-Carballo P, Kruszynska K, Repp C, et al. Secondary cell wall polymers of *Enterococcus faecalis* are critical for resistance to complement activation via mannose-binding lectin. *J Biol Chem.* 2012;287(45):37769-37777. doi: 10.1074/jbc.M112.358283. pmid: 22908219.
8. Teng F, Jacques-Palaz KD, Weinstock GM, Murray BE. Evidence that the enterococcal polysaccharide antigen gene (epa) cluster is widespread in *Enterococcus faecalis* and influences resistance to phagocytic killing of *E. faecalis*. *Infect Immun.* 2002;70(4):2010-2015. pmid: 11895965.
9. Thurlow LR, Thomas VC, Hancock LE. Capsular polysaccharide production in *Enterococcus faecalis* and contribution of CpsF to capsule serospecificity. *J Bacteriol.* 2009;191(20):6203-6210. doi: 10.1128/JB.00592-09. pmid: 19684130.
10. Aine E, Morsky P. Lysozyme concentration in tears--assessment of reference values in normal subjects. *Acta Ophthalmol (Copenh).* 1984;62(6):932-938. pmid: 6395619.
11. Hankiewicz J, Swierczek E. Lysozyme in human body fluids. *Clin Chim Acta.* 1974;57(3):205-209. pmid: 4434640.
12. Callewaert L, Michiels CW. Lysozymes in the animal kingdom. *J Biosci.* 2010;35(1):127-160. pmid: 20413917.
13. Herbert S, Bera A, Nerz C, Kraus D, Peschel A, Goerke C, et al. Molecular basis of resistance to muramidase and cationic antimicrobial peptide activity of lysozyme in staphylococci. *PLoS Pathog.* 2007;3(7):e102. pmid: 17676995.
14. Ibrahim HR, Thomas U, Pellegrini A. A helix-loop-helix peptide at the upper lip of the active site cleft of lysozyme confers potent antimicrobial activity with membrane permeabilization action. *J Biol Chem.* 2001;276(47):43767-43774. doi: 10.1074/jbc.M106317200. pmid: 11560930.
15. Hebert L, Courtin P, Torelli R, Sanguinetti M, Chapot-Chartier MP, Auffray Y, et al. *Enterococcus faecalis* constitutes an unusual bacterial model in lysozyme resistance. *Infect Immun.* 2007;75(11):5390-5398. doi: IAI.00571-07 [pii] 10.1128/IAI.00571-07. pmid: 17785473.
16. Benachour A, Ladjouzi R, Le Jeune A, Hebert L, Thorpe S, Courtin P, et al. The lysozyme-induced peptidoglycan *N*-acetylglucosamine deacetylase PgdA (EF1843) is required for *Enterococcus faecalis* virulence. *J Bacteriol.* 2012;194(22):6066-6073. doi: 10.1128/JB.00981-12. pmid: 22961856.
17. Fabretti F, Theilacker C, Baldassarri L, Kaczynski Z, Kropec A, Holst O, et al. Alanine esters of enterococcal lipoteichoic acid play a role in biofilm formation and resistance to antimicrobial peptides. *Infect Immun.* 2006;74(7):4164-4171. doi: 10.1128/IAI.00111-06. pmid: 16790791.

EPA decoration is essential for virulence

- 600 18. Benachour A, Muller C, Dabrowski-Coton M, Le Breton Y, Giard JC, Rince A, et al. The
601 *Enterococcus faecalis* sigV protein is an extracytoplasmic function sigma factor contributing to
602 survival following heat, acid, and ethanol treatments. J Bacteriol. 2005;187(3):1022-1035. doi:
603 187/3/1022 [pii] 10.1128/JB.187.3.1022-1035.2005. pmid: 15659680.
- 604 19. Le Jeune A, Torelli R, Sanguinetti M, Giard JC, Hartke A, Auffray Y, et al. The
605 extracytoplasmic function sigma factor SigV plays a key role in the original model of lysozyme
606 resistance and virulence of *Enterococcus faecalis*. PLoS ONE. 2010;5(3):e9658. doi:
607 10.1371/journal.pone.0009658. pmid: 20300180.
- 608 20. McKenzie HA, White FH, Jr. Determination of lysozyme activity at low levels with emphasis on
609 the milk enzyme. Anal Biochem. 1986;157(2):367-374. pmid: 3777441.
- 610 21. Zhang X, Paganelli FL, Bierschenk D, Kuipers A, Bonten MJ, Willems RJ, et al. Genome-wide
611 identification of ampicillin resistance determinants in *Enterococcus faecium*. PLoS Genet.
612 2012;8(6):e1002804. doi: 10.1371/journal.pgen.1002804. pmid: 22761597.
- 613 22. Palmer KL, Godfrey P, Griggs A, Kos VN, Zucker J, Desjardins C, et al. Comparative genomics
614 of enterococci: variation in *Enterococcus faecalis*, clade structure in *E. faecium*, and defining
615 characteristics of *E. gallinarum* and *E. casseliflavus*. MBio. 2012;3(1):e00318-00311. doi:
616 10.1128/mBio.00318-11. pmid: 22354958.
- 617 23. Dale JL, Cagnazzo J, Phan CQ, Barnes AM, Dunny GM. Multiple roles for *Enterococcus*
618 *faecalis* glycosyltransferases in biofilm-associated antibiotic resistance, cell envelope integrity,
619 and conjugative transfer. Antimicrob Agents Chemother. 2015;59(7):4094-4105. doi:
620 10.1128/AAC.00344-15. pmid: 25918141.
- 621 24. Rigottier-Gois L, Madec C, Navickas A, Matos RC, Akary-Lepage E, Mistou MY, et al. The
622 surface rhamnopolysaccharide epa of *Enterococcus faecalis* is a key determinant of intestinal
623 colonization. J Infect Dis. 2015;211(1):62-71. doi: 10.1093/infdis/jiu402. pmid: 25035517.
- 624 25. Hancock LE, Gilmore MS. The capsular polysaccharide of *Enterococcus faecalis* and its
625 relationship to other polysaccharides in the cell wall. Proc Natl Acad Sci U S A.
626 2002;99(3):1574-1579. doi: 10.1073/pnas.032448299 99/3/1574 [pii]. pmid: 11830672.
- 627 26. Briandet R, Meylheuc T, Maher C, Bellon-Fontaine MN. *Listeria monocytogenes* Scott A: cell
628 surface charge, hydrophobicity, and electron donor and acceptor characteristics under different
629 environmental growth conditions. Appl Environ Microbiol. 1999;65(12):5328-5333. pmid:
630 10583984.
- 631 27. Prajsnar TK, Renshaw SA, Ogryzko NV, Foster SJ, Serror P, Mesnage S. Zebrafish as a novel
632 vertebrate model to dissect enterococcal pathogenesis. Infect Immun. 2013;81(11):4271-4279.
633 doi: 10.1128/IAI.00976-13. pmid: 24002065.
- 634 28. Salamaga B, Prajsnar TK, Jareno-Martinez A, Willemse J, Bewley MA, Chau F, et al. Bacterial
635 size matters: Multiple mechanisms controlling septum cleavage and diplococcus formation are
636 critical for the virulence of the opportunistic pathogen *Enterococcus faecalis*. PLoS Pathog.
637 2017;13(7):e1006526. doi: 10.1371/journal.ppat.1006526. pmid: 28742152.
- 638 29. Giaouris E, Briandet R, Meyrand M, Courtin P, Chapot-Chartier MP. Variations in the degree of
639 D-Alanylation of teichoic acids in *Lactococcus lactis* alter resistance to cationic antimicrobials
640 but have no effect on bacterial surface hydrophobicity and charge. Appl Environ Microbiol.
641 2008;74(15):4764-4767. doi: 10.1128/AEM.00078-08. pmid: 18539809.
- 642 30. Dale JL, Nilson JL, Barnes AMT, Dunny GM. Restructuring of *Enterococcus faecalis* biofilm
643 architecture in response to antibiotic-induced stress. NPJ Biofilms Microbiomes. 2017;3:15. doi:
644 10.1038/s41522-017-0023-4. pmid: 28685097.
- 645 31. Teng F, Singh KV, Bourgoigne A, Zeng J, Murray BE. Further characterization of the epa gene
646 cluster and Epa polysaccharides of *Enterococcus faecalis*. Infect Immun. 2009;77(9):3759-3767.
647 doi: 10.1128/IAI.00149-09. pmid: 19581393.
- 648 32. Dunny GM, Brown BL, Clewell DB. Induced cell aggregation and mating in *Streptococcus*
649 *faecalis*: evidence for a bacterial sex pheromone. Proc Natl Acad Sci U S A. 1978;75(7):3479-
650 3483. pmid: 98769.
- 651 33. Talaga P, Vialle S, Moreau M. Development of a high-performance anion-exchange
652 chromatography with pulsed-amperometric detection based quantification assay for
653 pneumococcal polysaccharides and conjugates. Vaccine. 2002;20(19-20):2474-2484. pmid:
654 12057602.

EPA decoration is essential for virulence

- 655 34. Ames BN. Assay of inorganic phosphate, total phosphate and phosphatases. *Methods in*
656 *Enzymology*. 1966;8:115-118. doi: [doi.org/10.1016/0076-6879\(66\)08014-5](https://doi.org/10.1016/0076-6879(66)08014-5).
- 657 35. Ho SN, Hunt HD, Horton RM, Pullen JK, Pease LR. Site-directed mutagenesis by overlap
658 extension using the polymerase chain reaction. *Gene*. 1989;77(1):51-59. pmid: 2744487.
- 659 36. Maguin E, Duwat P, Hege T, Ehrlich D, Gruss A. New thermosensitive plasmid for gram-
660 positive bacteria. *J Bacteriol*. 1992;174(17):5633-5638. pmid: 1324906.
- 661 37. Mesnage S, Chau F, Dubost L, Arthur M. Role of *N*-acetylglucosaminidase and *N*-
662 acetylmuramidase activities in *Enterococcus faecalis* peptidoglycan metabolism. *J Biol Chem*.
663 2008;283(28):19845-19853. doi: M802323200 [pii] 10.1074/jbc.M802323200. pmid: 18490448.
- 664 38. Nusseim-Volhard CDR. *Zebrafish. A practical approach*. New York, NY: Oxford University
665 Press; 2002.

666

EPA decoration is essential for virulence

668 **Table 1. MIC of lysozyme for Firmicutes.**

Strain	lysozyme MIC (mg ml ⁻¹)	
<i>Staphylococcus aureus</i> COL	>16	669
<i>Streptococcus gallolyticus</i> UCN34	>16	670
<i>Streptococcus gordonii</i> DL-1 Challis	>16	671
<i>Streptococcus mutans</i> UA159	>16	672
<i>Enterococcus faecium</i> DO	>16	673
<i>Enterococcus hirae</i> ATCC9790	>16	674
<i>Enterococcus faecalis</i> OG1RF	>16	675
<i>Enterococcus faecalis</i> O (Δ oatA)	>16	676
<i>Enterococcus faecalis</i> OP (Δ oatA Δ pgdA)	16	677
<i>Enterococcus faecalis</i> OPD (Δ oatA Δ pgdA Δ dltA)	8	678
<i>Enterococcus faecalis</i> OPDV (Δ oatA Δ pgdA Δ dltA Δ sigV)	0.5	679
<i>Listeria monocytogenes</i> EGD	4	680
<i>Listeria monocytogenes</i> EGD Δ pgdA	0.125	681
<i>Lactococcus lactis</i> MG1363	0.125	682
<i>Bacillus subtilis</i> 168	0.0312	683
<i>Bacillus megaterium</i> KM	0.0312	684
<i>Lactobacillus cellobiosus</i> ATCC11739	0.0312	685
<i>Aerococcus viridans</i> ATCC11563	0.0312	686
<i>Micrococcus luteus</i> ATCC4698	0.0005	687

688

689 **Table 2. Complementation of *epa* transposon mutants.**

690

Mutant	Complementation gene			
	OG1RF_11720	OG1RF_11715	OG1RF_11714	OG1RF_11707
OPDV_11720::Tn2.9	+	ND	ND	ND
OPDV_11720::Tn2.5	+	-	-	-
OPDV_11715::Tn2.10	ND	+	ND	ND
OPDV_11715::Tn2.13	-	+	-	-
OPDV_11715::Tn2.16	-	+	-	-
OPDV_11714::Tn2.14	-	-	+	-
OPDV_11720::Tn2.12	ND	ND	ND	+
OPDV_11720::Tn2.8	ND	ND	-	+
OPDV_11720::Tn2.6	ND	ND	ND	+

691 ^a, Complementation was assessed on BHI-agar plates containing lysozyme at a concentration
692 of 0.5 mg ml⁻¹

693 +, complementation restoring lysozyme sensitivity; -, no impact on lysozyme MIC;

694 ND, not determined.

695

696

697 **Figure legends**

698

699 **Figure 1. Identification of *epa* mutants resistant to lysozyme. A.** Description of individual
700 transposon insertions. **B.** Mapping of transposon insertions in the *epa* variable region.
701 Insertion sites are indicated by vertical arrows. ORFs in the *epa* variable region are depicted
702 in grey. ²

703 **Figure 2. Growth defect of *E. faecalis* Tn mutants in the presence of antimicrobials**
704 **targeting the cell envelope.** Cell suspensions were prepared as described in S1 Fig and
705 1.5 μ l of serial dilutions were spotted on BHI-agar plates containing 10 ng ml⁻¹
706 anhydrotetracycline and various concentrations of lysozyme. Concentrations showing a clear
707 difference in susceptibility are shown.

708 **Figure 3. Analysis of purified EPA polysaccharides and their contribution to cell**
709 **surface charge. A.** Analysis of purified EPA by acrylamide gel electrophoresis. 40 μ g of
710 material was loaded on a 10 % (v/v) acrylamide-bisacrylamide (33:0.8) gel and stained with
711 the cationic dye alcian blue. **B.** Electrophoretic mobility of *E. faecalis* OG1RF, *OPDV* and
712 insertion mutants resistant to lysozyme. Representative mutants harbouring a transposon
713 insertion in *OG1RF_11720* (*OPDV_11720::Tn2.5*), *OG1RF_11715* (*OPDV_11715::Tn2.13*),
714 *OG1RF_11714* (*OPDV_11714::Tn2.14*) or *OG1RF_11707* (*OPDV_11707::Tn2.8*) were
715 analysed. Wild-type OG1RF and parental *OPDV* strains were included as controls. **C.**
716 Phosphate content of purified EPAs. 120 μ l of each purified polysaccharide at a
717 concentration of 1 mg ml⁻¹ was assayed as described previously [34]. **D.** Carbohydrate
718 composition of purified EPA polysaccharides. The relative percentage corresponding to each
719 monosaccharide was determined from three independent extractions.

720 **Figure 4. Structural analysis of purified EPA polysaccharides. A.** 1D proton spectra of
721 the EPA polysaccharides extracted from strains *OPDV*, *OPDV_11720::Tn2.5*,
722 *OPDV_11715::Tn2.13*, *OPDV_11714::Tn2.14* or *OPDV_11707::Tn2.8*. The grey boxes
723 indicate anomeric (4.5-5.5 ppm) and methyl protons (1.2-2.5 ppm). **B.** 2D ¹H-¹³C HSQC
724 spectra of EPA polysaccharides. The region corresponding to anomeric protons (4.2-5.5 ppm)
725 and anomeric carbons (90-105 ppm) is shown. *OPDV* signals are in black, mutant signals in
726 red. Boxes show signals with a lower intensity or a shift in the mutant EPA samples. Close-
727 up views of the boxed regions are shown in S4 Fig.

EPA decoration is essential for virulence

728 **Figure 5. Growth defect of *E. faecalis* OG1RF in frame *epa* mutants in the presence of**
729 **antimicrobials targeting the cell envelope.** Cell suspensions were prepared as described in
730 S1 Fig and 1.5 μ l of serial dilutions were spotted on BHI-agar plates containing 10 ng ml⁻¹
731 anhydrotetracycline and SDS, sodium cholate, polymyxin B or nisin. For each antimicrobial,
732 one concentration showing a difference in susceptibility is shown.

733 **Figure 6. Virulence of *epa* mutants and complemented strains in the zebrafish model of**
734 **infection.** Survival of zebrafish larvae (n>20) following infection with *E. faecalis* OG1RF
735 (WT) and *epa* deletion mutants was monitored over 90 h post infection. **A.** Mutant $\Delta I1720$.
736 **B.** Mutant $\Delta I1715$. **C.** Mutant $\Delta I1714$. **(D),** Mutant $\Delta I1707$. **E.** Statistical significance
737 determined by Log-rank test; ns, $P>0.05$; ** $P<0.01$; *** $P<0.001$; **** $P<0.0001$. All
738 injections presented in Fig 4A and 4D were carried out on the same day. The same data
739 corresponding to the OG1RF strain are therefore shown for the 2 experiments.

740 **Fig 7 *epaX* mutant cells are more prone to phagocytosis than wild-type and**
741 **complemented cells. A.** Quantification of *E. faecalis* uptake by zebrafish phagocytes.
742 Embryos were infected with 1,600 CFUs of *E. faecalis* cells constitutively producing
743 mCherry and fixed in 4 % paraformaldehyde 1.5 h post infection. Phagocytes were
744 immunolabelled using rabbit anti L-plastin antibodies and detected with goat anti-rabbit
745 antibodies conjugated to Alexafluor 488. The infected and immunolabelled embryos were
746 imaged using scanning confocal microscope. The ratio of mCherry fluorescence signal area
747 associated with phagocytosed and free bacteria was measured using the Fish Analysis Fiji
748 plugin. The uptake of mutant OG1RF $\Delta I1714$ ($\Delta epaX$) was significantly higher when
749 compared to the wild-type (OG1RF; *** $P = 0.0006$) and complemented strain (OG1RF
750 $\Delta I1714 + pTetH-OG1RF_{11714}$; ** $P = 0.0049$). No difference in phagocytosis was
751 observed between the wild-type and complemented strains (ns, $P>0.05$). Representative
752 images showing *E. faecalis* uptake in zebrafish embryos are shown. Each picture corresponds
753 to the quantification result indicated with a red dot in **A**, following infection with OG1RF
754 **(B)**, OG1RF $\Delta I1714$ ($\Delta epaX$) **(C)** and the complemented strain **(D)**. Phagocytes labeled with
755 L-plastin appear in green, mCherry labelled bacteria in red. Scale bar is 25 μ m.

756

757

758

759 **Supporting information Legend**

760 **S1 Figure. Lysozyme MICs for Firmicutes.** A cell suspension in phosphate saline buffer
761 was adjusted to an OD at 600 nm of 1 and 1.5 μ l of serial dilutions were spotted on BHI-agar
762 plates containing various concentrations of lysozyme. ND, undiluted cell suspension; 10^{-1} ,
763 10-fold dilution; 10^{-2} , 100-fold dilution; 10^{-3} , 1000-fold dilution; 10^{-4} , 10000-fold dilution;
764 10^{-5} , 100000-fold dilution.

765 **S2 Figure. Western blot analysis of complementation strains.** Cultures were grown in BHI
766 to an OD at 600 nm of 0.5 and expression of the *epa* genes was induced by addition of
767 anhydrotetracycline (10 ng ml^{-1}). After 2 h, cells were harvested and mechanically broken in
768 the presence of glass beads. Crude extracts ($20 \mu\text{g}$) were loaded on SDS-PAGE, transferred
769 onto a nitrocellulose membrane and probed with a polyclonal serum against the polyhistidine
770 tag. Bands of the expected molecular weights were detected (OG1RF_11707, 36.7 kDa;
771 OG1RF_11714, 38.9 kDa; OG1RF_11715, 38.4 kDa; OG1RF_11720, 30.8 kDa).

772 **S3 Figure. HPLC analysis of TFA-hydrolysed EPA polysaccharides.** Following gel
773 filtration, fractions containing neutral sugars were pooled and freeze-dried. EPA was
774 hydrolysed in the presence of 4 N TFA at 100°C for 4 h. Monosaccharides were separated on
775 a carbopac PA10 column by high performance anion exchange chromatography coupled to
776 pulsed-amperometric detection. Representative chromatograms are shown for
777 monosaccharide standards and each transposon mutant. EPA polysaccharides were extracted
778 from three independent cultures to give average values in Fig 3D.

779 **S4 Figure. ^1H - ^{13}C HSQC spectra showing signals altered in *epa* mutants. A.** Region
780 corresponding to anomeric protons (4.2-5.5 ppm) and anomeric carbons (90-105 ppm)
781 highlighting four regions of the spectra (boxed) with signals shifted or changing in intensity
782 in the *epa* mutants. **B.** Boxed regions in A. are shown for individual mutant and one
783 complemented strain.

784 **S5 Figure. PCR analysis of OG1RF derivatives harbouring in-frame deletions in**
785 ***OG1RF_11720*, *OG1RF_11715*, *OG1RF_11714* and *OG1RF_11707*.**

786 **S6 Figure. Virulence of *epa* transposon mutants and complemented strains in the**
787 **zebrafish model of infection.** Survival of zebrafish larvae ($n > 20$) following infection with *E.*
788 *faecalis* OG1RF (WT) and *epa* insertion mutant was monitored over 90h post infection.
789 **A.** Mutant *OPDV_11720::Tn2.5*. **B.** Mutant *OPDV_11715::Tn2.13*. **C.** Mutant

EPA decoration is essential for virulence

790 *OPDV_11714::Tn2.14*. **D.** Mutant *OPDV_11707::Tn2.8*. Statistical significance was
791 determined by Log-rank test; NS, $P>0.05$; ** $P<0.01$; *** $P<0.001$; **** $P<0.0001$. The
792 same data corresponding to the WT strain are shown in Fig4A/4C and Fig 4B/4D.

793 **S7 Figure. Comparative analysis of OG1RF and *OPDV* virulence in the zebrafish model**
794 **of infection.** Survival of zebrafish larvae (n=28) following infection with 1,000 CFUs of *E.*
795 *faecalis* OG1RF (WT) and *OPDV* mutant was monitored over 90 h post infection. The lack of
796 statistical significance ($P=0.645$) was determined by Log-rank test.

797 **S8 Figure. Growth rate analysis of *E. faecalis* OG1RF and *epa* derivatives.** Cells from
798 overnight cultures in BHI were diluted to an OD at 600 nm of 0.01 in 25 ml BHI and growth
799 of standing cultures was monitored over 6 h. The data presented are the average of 3
800 independent cultures. The same OG1RF growth curves were used as a control in each graph.

801 **S9 Figure. Step-by-step description of the transposon mapping strategy.** **A.** Schematic
802 representation of the *mariner* transposon used. It consists of a gentamycin resistance cassette
803 flanked by two inverted repeats. **B.** Step 1: digestion of chromosomal DNA with SspI, which
804 has a unique cleavage site in the gentamycin resistance cassette. **C.** step 2: self-ligation of
805 SspI digestion products. **D.** step 3: reverse PCR on ligation products with two divergent
806 oligonucleotides (Mar_dn and Mar_up). **E.** step 4: sequencing of the PCR product using
807 oligonucleotide T7.

808
809 **S1 Table. Electrophoretic mobility measurements.** The values presented are the average of
810 three independent biological replicates \pm standard deviation.

811
812 **S2 Table. Statistical significance of pairwise comparisons of electrophoretic mobility.**
813 The significance values have been calculated using two-way ANOVA.

814
815 **S3 Table. Statistical significance of pairwise comparisons of phosphate assays.** The
816 significance values have been calculated using unpaired t-test.

817
818 **S4 Table. Bacterial strains, plasmids and oligonucleotides used in this study.**

A

Disrupted gene ^a	Insertion site	Mutant	Gene	Putative function
<i>OG1RF_11720</i> (<i>EF2176</i>)	nt 392 of 759	<i>OPDV_11720::Tn2.9</i>	<i>cpsH</i> ^b	Glycosyl transferase
<i>OG1RF_11720</i> (<i>EF2176</i>)	nt 619 of 759	<i>OPDV_11720::Tn2.5</i>	<i>cpsH</i>	Glycosyl transferase
<i>OG1RF_11715</i> (<i>EF2170</i>) ^c	nt 43 of 978	<i>OPDV_11715::Tn2.10</i>	<i>epaOX</i>	Glycosyl transferase
<i>OG1RF_11715</i> (<i>EF2170</i>)	nt 553 of 978	<i>OPDV_11715::Tn2.13</i>	<i>epaOX</i>	Glycosyl transferase
<i>OG1RF_11715</i> (<i>EF2170</i>)	nt 925 of 978	<i>OPDV_11715::Tn2.16</i>	<i>epaOX</i>	Glycosyl transferase
<i>OG1RF_11714</i> (<i>EF2170</i>) ^d	nt 478 of 981	<i>OPDV_11714::Tn2.14</i>	<i>epaX-like</i>	Glycosyl transferase
<i>OG1RF_11707</i> (<i>EF2165</i>)	50nt upstream ATG	<i>OPDV_11707::Tn2.12</i>	<i>rfbB</i> ^e	Epimerase/dehydratase
<i>OG1RF_11707</i> (<i>EF2165</i>)	24nt upstream ATG	<i>OPDV_11707::Tn2.8</i>	<i>rfbB</i>	Epimerase/dehydratase
<i>OG1RF_11707</i> (<i>EF2165</i>)	nt 828 of 951	<i>OPDV_11707::Tn2.6</i>	<i>rfbB</i>	Epimerase/dehydratase

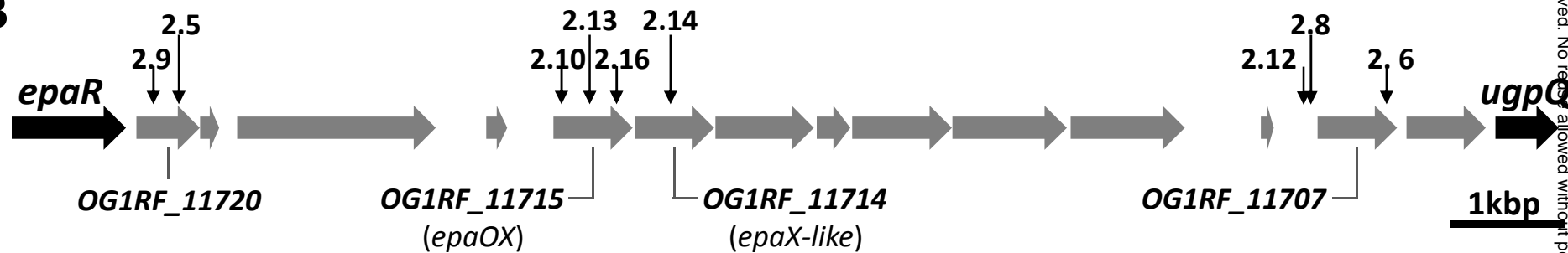
^a The closest homolog in *E. faecalis* V583 is indicated in brackets

^b *OG1RF_11720* is 99.7 % identical to *Streptococcus pneumoniae cpsH*

^c *OG1RF_11715* shares 28 % identity and 45 % similarity with *EF2170*

^d *OG1RF_11714* shares 53 % identity and 61 % similarity with *EF2170*

^e *OG1RF_11707* is 100 % identical to *S. pneumoniae rfbB*

B**Figure 1**

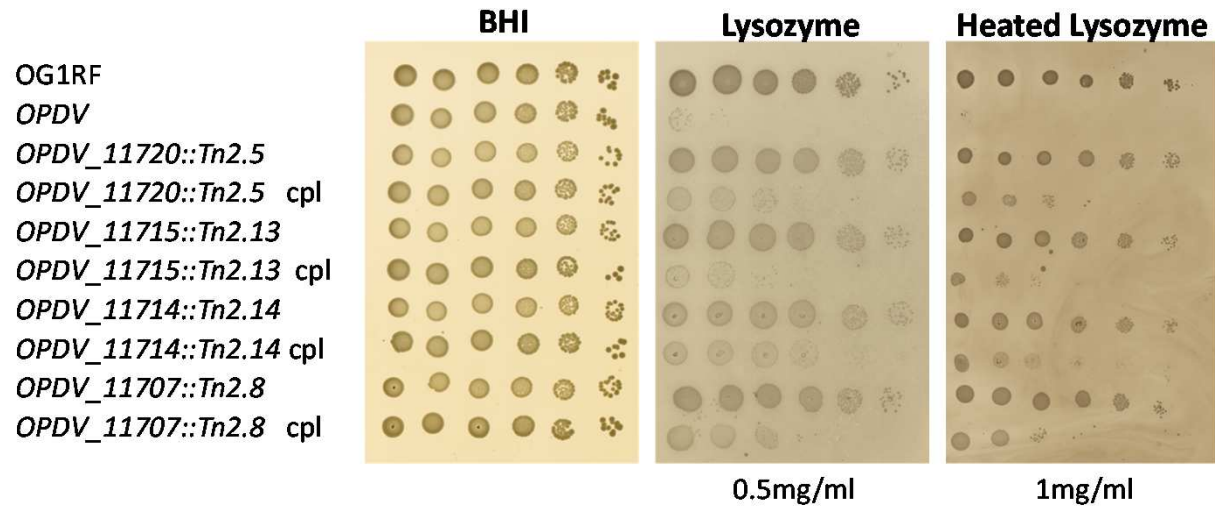


Figure 2

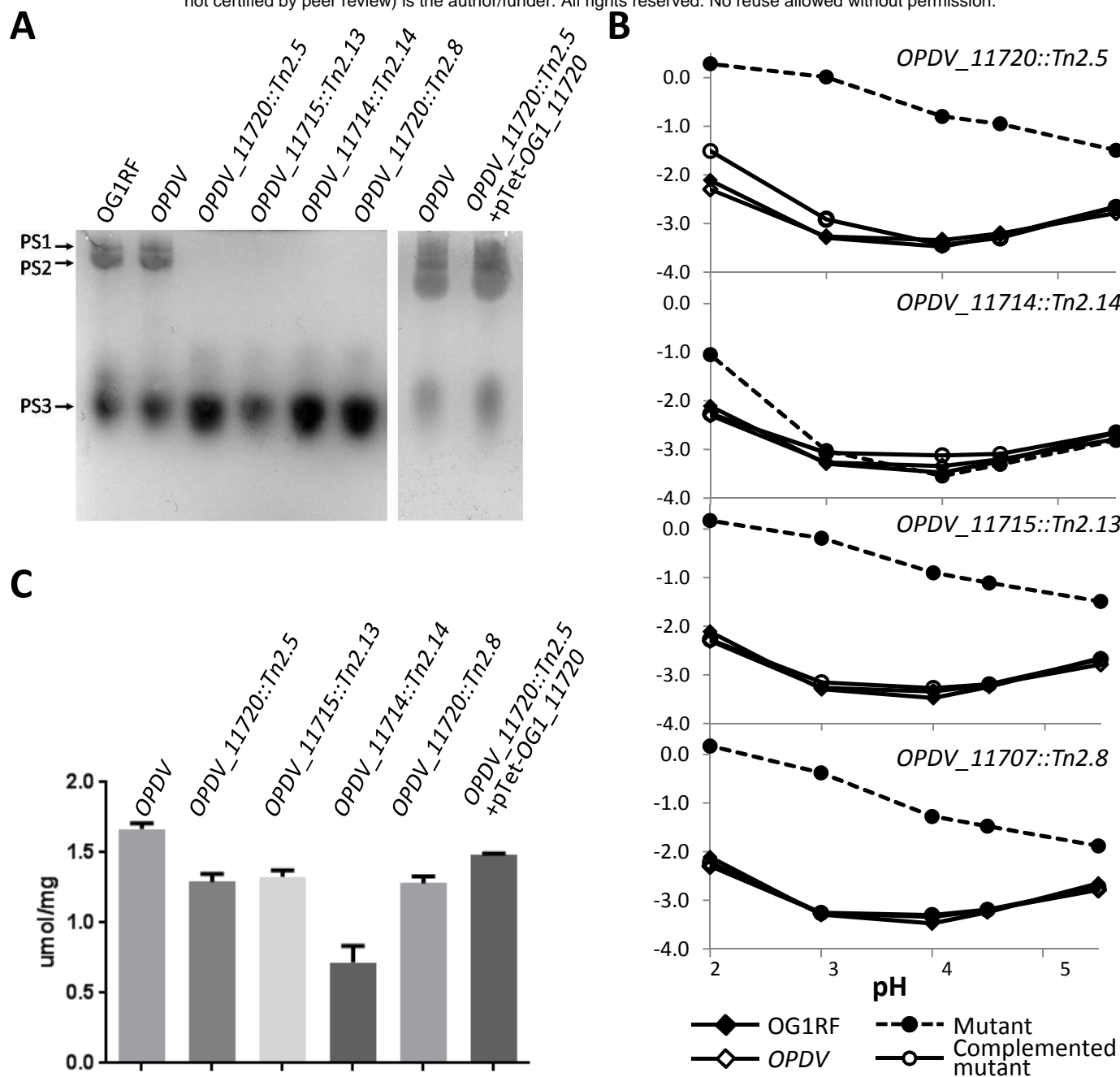
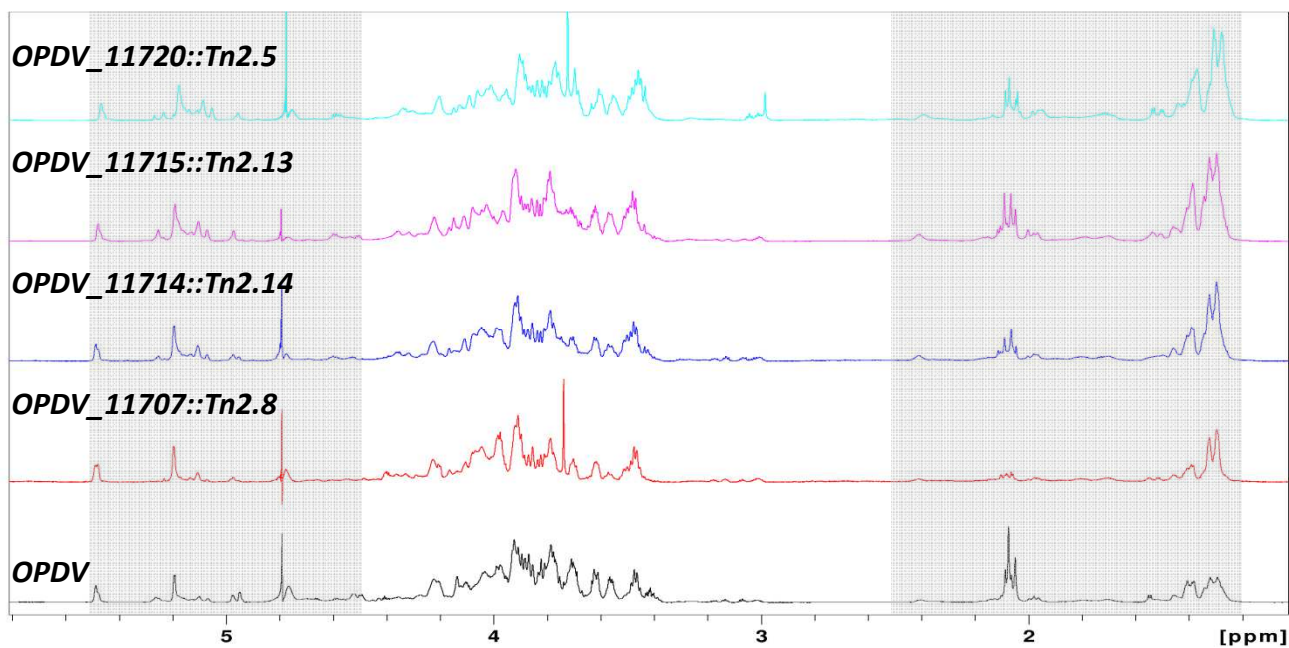


Figure 3

A



B

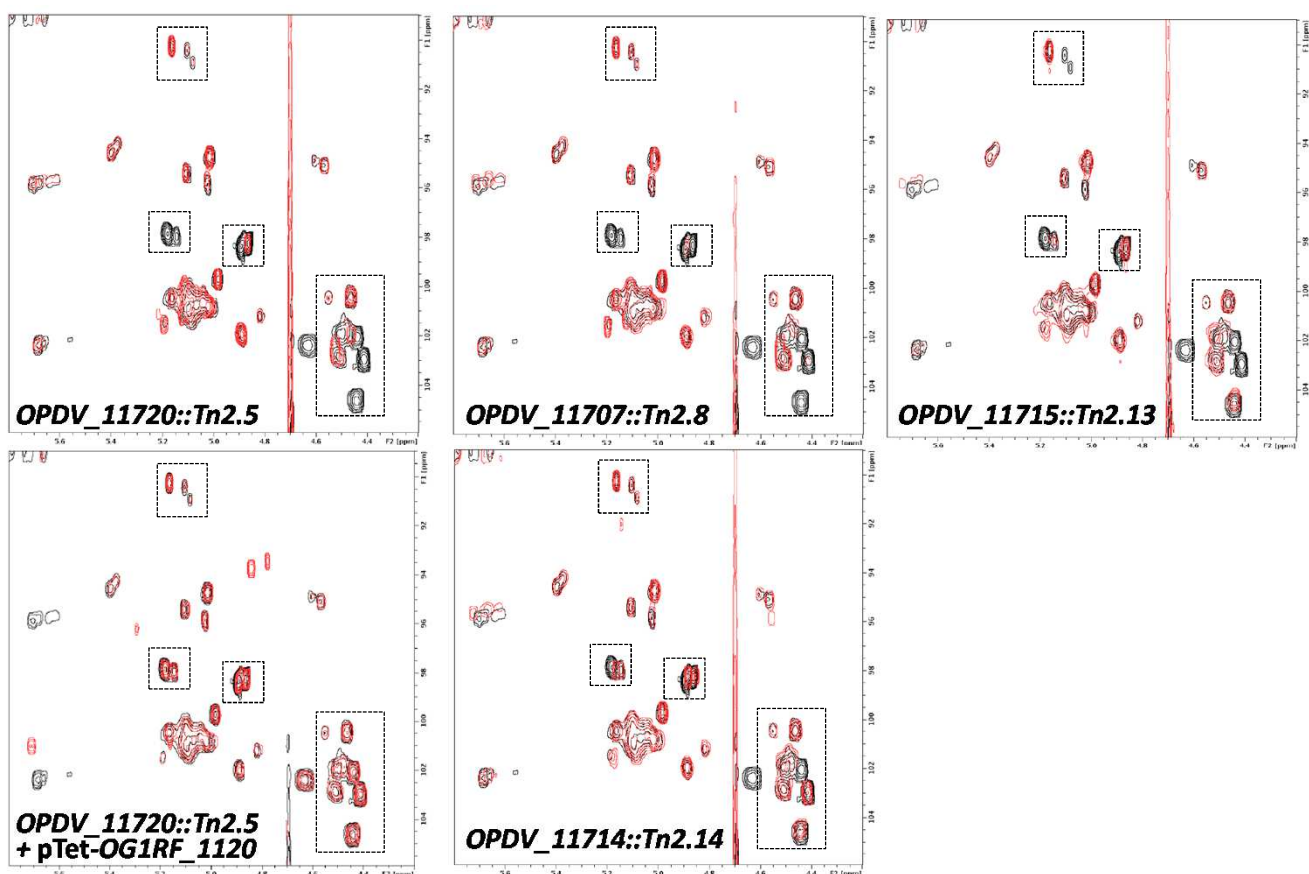


Figure 4

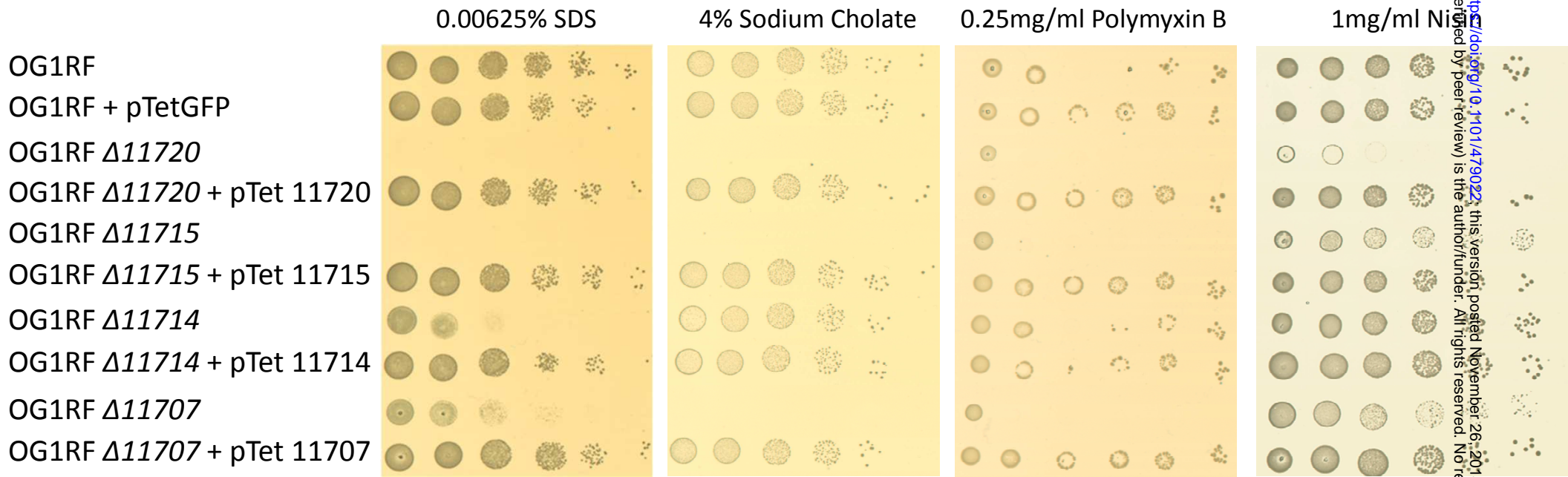
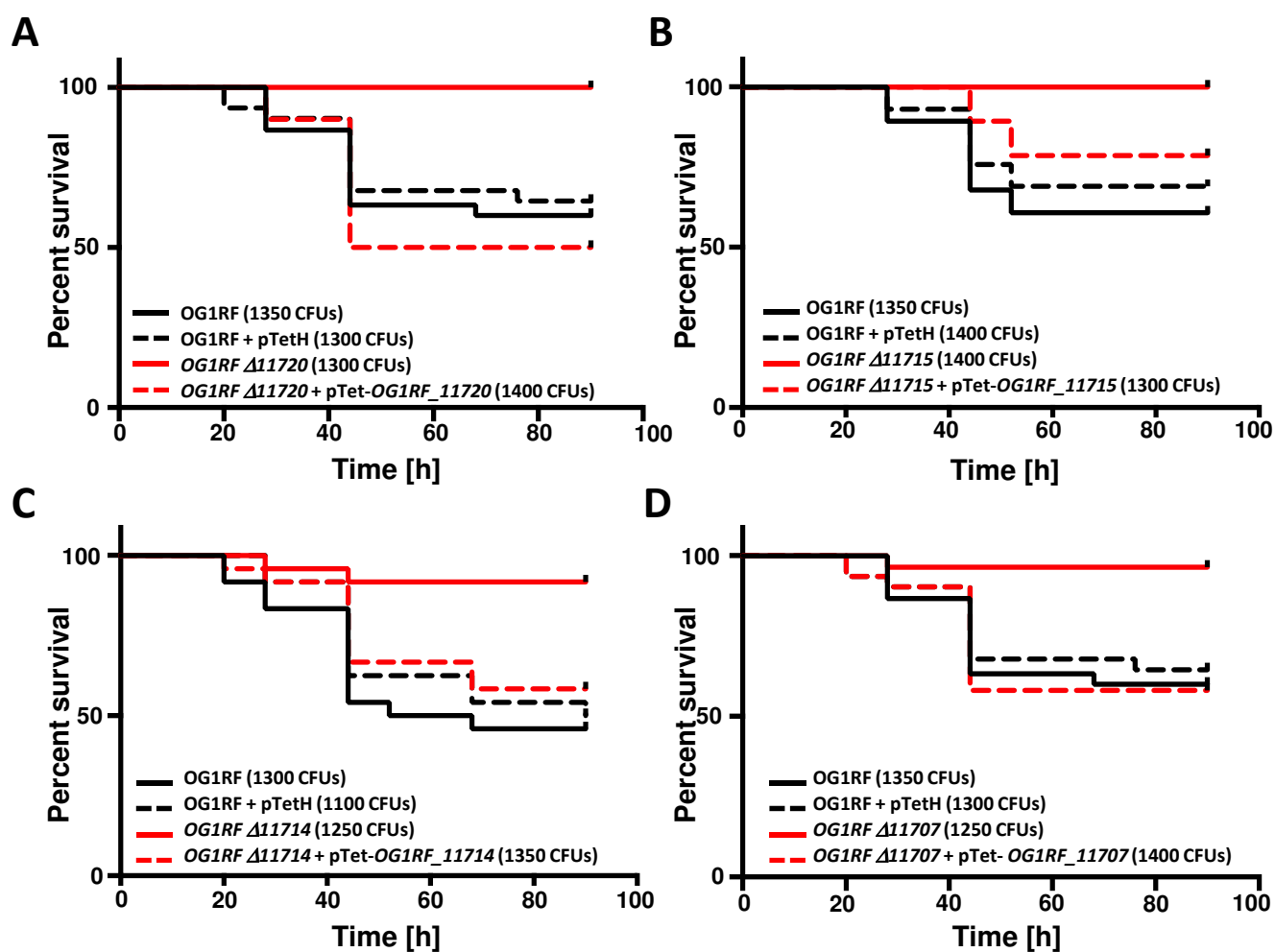


Figure 5



	Significance	P value
OG1RF vs OG1RF + pTetH	ns	0.7158
OG1RF vs OG1RF Δ 11720	****	<0.0001
OG1RF + pTetH vs OG1RF Δ 11720 + pTet-OG1RF_11720	ns	0.3095
OG1RF Δ 11720 vs OG1RF Δ 11720 + pTet-OG1RF_11720	****	<0.0001
OG1RF vs OG1RF + pTetH	ns	0.4985
OG1RF vs OG1RF Δ 11715	***	0.0001
OG1RF + pTetH vs OG1RF Δ 11715 + pTet-OG1RF_11715	ns	0.3501
OG1RF Δ 11715 vs OG1RF Δ 11715 + pTet-OG1RF_11715	**	0.0079
OG1RF vs OG1RF + pTetH	ns	0.6021
OG1RF vs OG1RF Δ 11714	***	0.0008
OG1RF + pTetH vs OG1RF Δ 11714 + pTet-OG1RF_11714	ns	0.6186
OG1RF Δ 11714 vs OG1RF Δ 11714 + pTet-OG1RF_11714	**	0.0099
OG1RF vs OG1RF + pTetH	ns	0.7158
OG1RF vs OG1RF Δ 11707	**	0.0012
OG1RF + pTetH vs OG1RF Δ 11707 + pTet-OG1RF_11707	ns	0.6321
OG1RF Δ 11707 vs OG1RF Δ 11707 + pTet-OG1RF_11707	***	0.0008

